Appl Phys A (2011) 102: 27–33
DOI 10.1007/s00339-010-6013-5

Applied Physics A
Materials Science & Processing

RAPID COMMUNICATION

Femtosecond laser interaction with pulsed-laser deposited carbon thin films of nanoscale thickness

M. Forster · L. Égerházi · C. Haselberger · C. Huber · W. Kautek

Received: 9 August 2010 / Accepted: 10 August 2010 / Published online: 27 August 2010

Abstract The dependence of optical, electronic and thermal penetration zones on the thickness of nanoscale layers grown on silicon wafers is reported. Tetrahedral amorphous carbon (ta-C) and amorphous carbon nitride (a-C_xN_y) films were prepared by inverse pulsed laser deposition (IPLD). Single-pulse modification thresholds for femtosecond laser processing proved to be dependent on the actual film thickness below 60 nm for ta-C and 90 nm for a-C_xN_y. The modification behaviour was governed by multiphoton processes. An effective penetration depth of the laser radiation in a-C_xN_y was of ca. 110 nm in accordance with two-photon absorption. Both the emergence length of ballistic hot electrons and the heat diffusion length are negligible in these thin film materials. The lower bulk value of the threshold fluence of the a-C_xN_y films as compared to ta-C is mainly controlled by optical contributions due to nitrogen-related defects.

1 Introduction

Ultrahigh precision femtosecond laser processing of materials represents a cutting-edge technology [1–3] in competition with electron [4, 5] and ion beam nano-structuring techniques [6]. In processing nanometer-thin films, not only the lateral but also—particularly—the vertical in-depth precision is decisive. The energy deposition by impacting electrons, ions, or by absorbed photons into such nanoscale materials must be limited to the respective film volume. Whereas electron beams exhibit ultimate lateral precision [7] of the order of several 10 nm, the vertically affected zone and therefore the resolution is only of several micrometres, highly dependent on the atomic number [8]. In contrast, ultimate nanoscale thermal diffusion control in femtosecond laser processing can minimise the vertical and lateral heat-affected zone (HAZ) down to the order of 10 nm, depending on the heat diffusivity and electron–phonon relaxation time of the respective material [1, 9, 10]. This outstanding property is one of the reasons for the breakthrough of fs-lasers in material machining [1, 11–15]. Near-infrared ultrashort laser pulses with durations of 5 fs yielded additional machining precision features based on nonlinear optical coupling and deterministic excitation effects [16–18].

In the regime of nanosecond-pulse laser interactions, the behaviour of the ablation threshold fluence is controlled by thermal conductivity processes, i.e. the HAZ or in other words the heat diffusion length, l_T, of the film material [1, 19, 20]:

$$l_T \approx \sqrt{D\tau_l}, \tag{1}$$

where D is the heat diffusivity of the lattice and τ_l the laser pulse duration. The ablation threshold fluence, F_{th}, of thin, thermally conducting films on thermally insulating substrates is lowered when the film thickness h becomes less than l_T ($h < l_T$). According to this model, F_{th} increases linearly with film thickness h for $h < l_T$ up to the point where $h = l_T$, as shown for nickel films processed with

M. Forster · L. Égerházi · C. Haselberger · C. Huber · W. Kautek (✉)
Department of Physical Chemistry, University of Vienna, Währinger Straße 42, 1090 Vienna, Austria
e-mail: wolfgang.kautek@univie.ac.at

L. Égerházi
Department of Optics and Quantum Electronics, University of Szeged, POB 406, 6701 Szeged, Hungary

L. Égerházi
Institute of Medical Physics and Biophysics, University of Szeged, Dóm tér 13, 6720 Szeged, Hungary

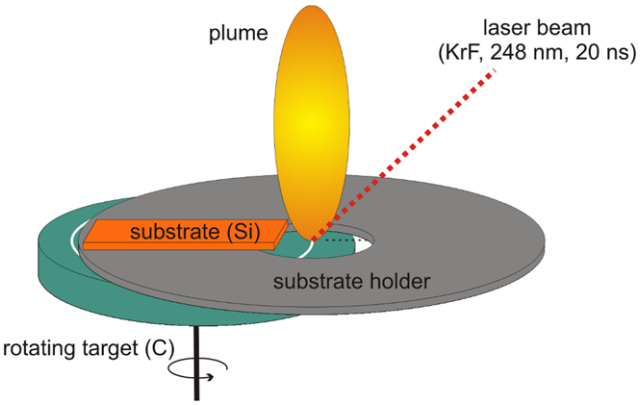

Fig. 1 Inverse pulsed laser deposition setup

14 ns pulses at 248 nm wavelength [21]. When $h > l_T$, F_{th} becomes independent of h and equal to the bulk material value [22]. Applying short pulse lengths of $\tau_l < 1$ ps, the longer electron–phonon relaxation time τ_e has to replace the pulse length τ_l in (1) [13, 15, 23, 24]:

$$l_T \approx \sqrt{D\tau_e}. \tag{2}$$

A thickness-dependent modification fluence threshold using fs-excitation was interpreted by the heat penetration depth within the electron gas before electron–phonon relaxation occurs with single- and multi-shot treatments of thin gold films on glass [25] and by the penetration depth of laser radiation with multi-pulse treatments of hydrogenated DLC (a-C:H) films grown by plasma-assisted chemical vapour deposition on glass [26].

In the present study of fs-laser materials processing, experimental modification fluence thresholds were used to characterise the interdependence of optical, electronic and thermal penetration zones with the thickness of nanoscale tetrahedral amorphous carbon, ta-C, and amorphous carbon nitride films, a-C_xN_y, grown on silicon wafers by inverse pulsed laser deposition (IPLD).

2 Experimental

Tetrahedral amorphous carbon films, ta-C, and amorphous carbon nitride films, a-C_xN_y, were prepared by inverse pulsed laser deposition (IPLD) (Fig. 1) [27]. The deposition chamber was first evacuated to a pressure of 1.5–2×10^{-4} Pa, which then was increased to 5 Pa by introducing high-purity Ar and N_2 gas (both 99.999%), respectively. A graphite target was rotated at 10 rpm and was ablated at 10 Hz repetition rate by KrF laser pulses (248 nm, 20 ns, 7 J cm^{-2}). The laser beam was focused by a 35 cm focal length lens onto a ~0.01 cm^2 area of the target surface at 45° angle of incidence [28]. Films were grown at room temperature on two 8 mm wide polished silicon stripes, fixed onto a substrate holder in the plane of the surface of the rotating target. The masked silicon stripes were positioned along the symmetry axes of the elliptical laser spot (static IPLD, Fig. 1). The thickness profiles of the layers were measured to be between 0 and 300 nm using profilometry. Samples with constant film thickness of 150 nm were deposited on small silicon substrates fixed to the surface of the graphite target within the circular ablation track (co-rotating IPLD, Fig. 1).

Using the IPLD setup, two types of films were generated: a tetrahydral amorphous carbon film, ta-C, and an amorphous carbon nitride film, a-C_xN_y (Ar and N_2 gases are introduced into the deposition chamber, respectively). The atmosphere in the growth chamber determines the film properties [29]. A nitrogen atmosphere of ≤ 1 Pa causes a minute influence on the stoichiometry, the density ($\rho > 3$ g cm^{-3}), the conductivity ($G < 0.01\ \Omega^{-1}$ cm^{-1}), and the bandgap $E_g \approx 1.8$ eV of the ta-C film [29]. When the nitrogen atmosphere is increased above 5 Pa, the stoichiometry rapidly changes from ta-C to a nitride type, a-C_xN_y accompanied by a replacement of C-sp^3 by C-sp^2 hybridization, resulting in a conductivity higher by four orders of magnitude, a much lower density ($\rho < 2.2$ g cm^{-3}) and increased roughness and porosity. A 5 Pa nitrogen pressure already results in a nitrogen atomic fraction of $y \approx 0.26$, a density of $\rho = 2.15$ g cm^{-3}, and a conductivity of $G \approx 335\ \Omega^{-1}$ cm^{-1}. In contrast, the ta-C type films deposited in argon atmosphere were classified to contain an sp^3 content of about 80% and thus could be described as ta-C [30]. One may associate the properties of this type with respective values of the a-C films grown in 10^{-5} Pa N_2 introduced in the deposition chamber as described before [29], where the stoichiometry of C is >96% with $G \approx 0.01\ \Omega^{-1}$ cm^{-1} and $E_g \approx 1.8$ eV (Table 2).

During the processing, the films were irradiated using a 60 fs high-power 11 MHz laser system employing fs-power-oscillator technology (Femtosource Scientific XL, Femtolasers Produktions GmbH, Vienna, Austria) and an 18 W pump laser. The centre wavelength was 790 nm and the bandwidth 30 nm. A Pockels cell served for single-pulse processing. The beam delivery was performed by an optical microscope (Zeiss Axio Imager.M1) equipped with an xyz translation stage, through a 63× and a 100× microscope objective (Neofluar) with a numerical aperture of NA = 0.75. Dispersions introduced were pre-compensated by chirped mirrors [31]. The pulse duration was directly determined after the objective of the microscope by autocorrelation and was found to be 60 fs. The maximum pulse energy was 205 nJ at the oscillator output and 120 nJ at the sample surface. The pulse energy was controlled by a combination of a polariser and a half-wave plate.

The irradiated areas were microscopically inspected online. Detailed morphological examinations were carried out by a scanning force microscope (SFM; NTEGRA AURA) in contact-mode.

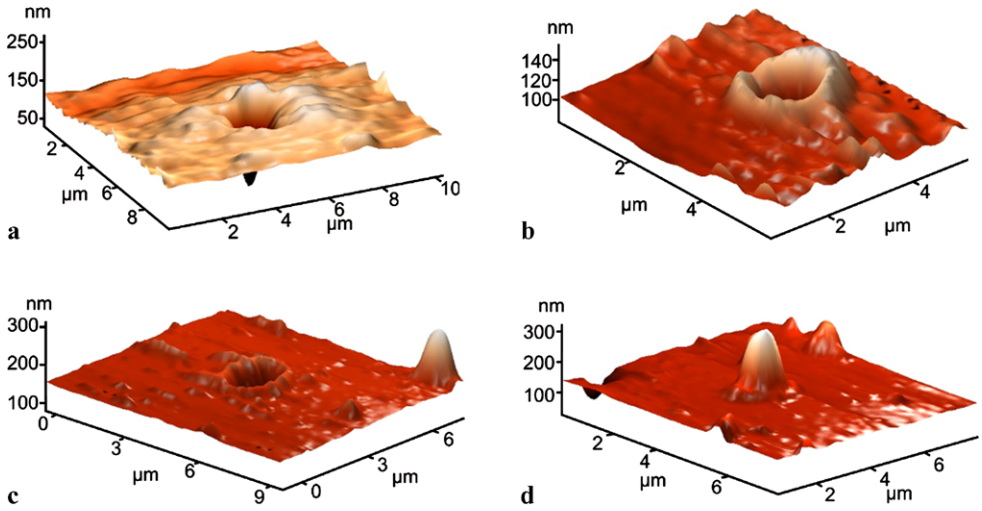

Fig. 2 Topographies of laser treated sites on a 150 nm thick ta-C layer. (**a**) $N = 2000$, $F = 0.48\ \mathrm{J\,cm^{-2}}$, (**b**) $N = 10$, $F = 0.28\ \mathrm{J\,cm^{-2}}$, (**c**) $N = 1$, $F = 0.42\ \mathrm{J\,cm^{-2}}$, (**d**) $N = 1$, $F = 0.28\ \mathrm{J\,cm^{-2}}$

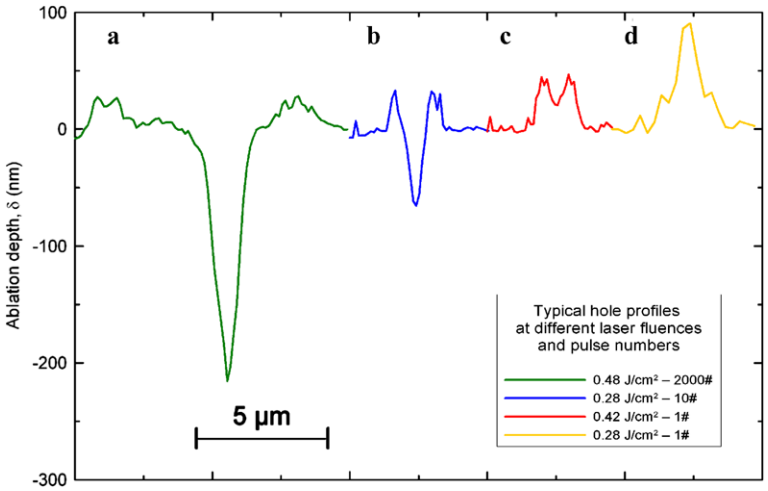

Fig. 3 Cross sections of SFM measurements for different modification zones (for parameters see Fig. 2) on a 150 nm thick ta-C film

3 Results and discussion

A 150 nm thick ta-C layer of constant thickness on a silicon substrate was exposed to laser pulses using different pulse energies, E, and different pulse numbers, N. The craters were evaluated optically with a widefield microscope and an SFM. Different topographies were observed and typical types of modifications are shown in Fig. 2 with their corresponding cross sections in Fig. 3. Using high pulse numbers and high fluences, F, deep ablation craters were observed which exceeded the IPLD layer thickness (>150 nm) (Fig. 3a). Processing with lower N and F (Fig. 3b and c) resulted in shallower craters with more pronounced rims above the surface level. At single-shot experiments with low F (Fig. 3d), a volume increase probably due to graphitisation processes with conversion of sp^3 to sp^2 hybridization followed by foaming can be observed (cf. [32, 33]). It follows from this incubation process that multi-pulse experiments are concerned with converted and graphitised material, and not with the pristine ta-C material. Therefore the dependence of F_{th} on the film thickness is only discussed for single-pulse treatments.

For high pulse numbers, an ablation threshold has been determined using the D^2–ln E relationship (Fig. 4). In this technique, the diameter of the modified zones, D, is plotted versus the logarithm of the pulse energy, E, yielding the Gauss radius, w_0, and the threshold energy, E_{th} [15]:

$$D^2 = 2w_0^2 \ln\left(\frac{E}{E_{th}}\right). \tag{3}$$

Precise maximum fluence values in the Gaussian profile, F_0, can be calculated from E:

$$F_0 = \frac{2E}{\pi w_0^2}. \tag{4}$$

For low pulse numbers ($N \leq 100$), a distinction between holes deeper than the original ta-C layer and shallow holes which do not penetrate the silicon substrate was made based on SFM depth measurements. The ablation thresholds of

Table 1 Modification thresholds for the silicon substrate and the ta-C layer at a constant thickness of 150 nm

	$F_{th}(N)$/J/cm^2
Silicon	
$N = 2000$	0.08
$N = 1000$	0.08
$N = 100$	0.12
$N = 10$	0.15
ta-C film	
$N = 100$	0.11
$N = 10$	0.12
$N = 1$	0.14

Table 2 Summary of parameters of DLC layers

	ta-C	a-C_xN_y	References
E_g [eV]	1.8	–	[29]
	2.5–3	~1	[41]
ρ [g cm^{-3}]	3	2.25	[29]
G [Ω^{-1} cm^{-1}]	0.01	335	[29]
F_{th} (bulk) [J cm^{-2}]	0.1–0.2	–	[41]
	0.12	0.065	This work
l_α ($\lambda = 310$ nm) [nm]	30	–	[30]
l_α ($\lambda = 400$ nm) [nm]	670	<330*	[37]
l_α ($\lambda = 800$ nm) [nm]	3000		[30]
	16,700	<5000*	[37]
l_α ($\lambda = 800$ nm) [nm]	–	110	This work
Number of photons	–	2	[37]

*Value for 12% nitrogen; for 26% nitrogen it is supposed to be lower

both the ta-C film and the Si-substrate (Fig. 4) have been determined (Table 1).

The relation between the single-pulse $F_{th}(1)$ and the multiple-pulse thresholds $F_{th}(N)$ can be described by the phenomenological model

$$F_{th}(N) = F_{th}(1) \cdot N^{\xi - 1}, \tag{5}$$

where the parameter ξ indicates the degree of incubation [15]. A value of $\xi = 1$ is indicative of the absence of incubation. From a plot using (5) and the threshold values in Fig. 4, an incubation factor of $\xi = 0.86$ was derived for the silicon substrate in good agreement with previous investigations ($\xi = 0.82$) [34].

Single-pulse ablation and modification thresholds of the a-C_xN_y and the ta-C films were determined using the D^2–ln E relationship in dependence of the film thickness (10–270 nm and 10–320 nm, respectively). Thickness-dependent modification thresholds were observed for ta-C films below 60 nm, and for a-C_xN_y samples below 90 nm (Fig. 5). The threshold fluences above these thicknesses are around 0.120 J cm^{-2} and 0.065 J cm^{-2}, respectively. The bulk threshold value of the ta-C film compares well with the value of 0.1–0.2 J cm^{-2} observed by a 40–150 fs laser treatment on bulk a-C:H films produced by unbalanced magnetron sputtering [35] and hot filament diode discharge [36].

Multi-pulse incubation leads to more or less strongly modified optical properties of DLC films (cf. $\xi = 0.86$) which cannot be correlated with pristine samples as e.g. at hydrogenated DLC (a-C:H) films grown by plasma-assisted chemical vapour deposition on glass [26]. Actually there, the single-pulse threshold was independent of the film thickness between 11 nm and 5.8 µm in contrast to the present results in Fig. 5.

Ablation threshold fluences of the thin films were determined by SFM and optical evaluation of the modification diameters and by the ablation rates, d, which are the absolute ablation depth quantified by SFM divided by the number of pulses per spot, N, vs. the logarithm of the fluence (results are included in Fig. 5) using

$$d = \frac{1}{\alpha_{eff}} \ln\left(\frac{F_0}{F_{th}}\right), \tag{6}$$

with an effective absorption coefficient α_{eff} [15] which is given by

$$\alpha_{eff} = \alpha_0 + \sigma_i N_i + \alpha_D(N) + \alpha_{NL}. \tag{7}$$

α_{eff} may include the linear temperature-dependent absorption coefficient of the pure material, α_0, a term $\sigma_i N_i$, caused by light absorbing impurities with a cross-section σ_i, a number per unit volume N_i, α_D, which takes into account changes in absorption caused by radiation-induced defects such as incubation centres as a function of N, and the multiphoton (nonlinear optical) absorption coefficient, α_{NL} [1].

One can assume that both examined phases exhibit a similar pure α_0 due to their identical production apart from the nitrogen addition in case of the a-C_xN_y film. The second term, $\sigma_i N_i$, will drastically contribute in the case of the high-nitrogen content species in contrast to the ta-C type. Incubation contribution needs not to be considered when using only $N = 1$, i.e. $\alpha_D = 0$. The nonlinear contribution, α_{NL}, will be discussed below. Thus, (7) reduces to

$$\alpha_{eff} \approx \alpha_0 + \sigma_i N_i + \alpha_{NL}. \tag{8}$$

The reciprocal value of α_{eff} is an effective penetration depth of energy density sufficient for evaporation (sublimation), $l_{eff} = \alpha_{eff}^{-1}$. In the simplest ansatz, F_{th} can be related to the sublimation energy volume density, E_{sub}, and l_{eff}:

$$F_{th} = E_{sub} \cdot l_{eff}. \tag{9}$$

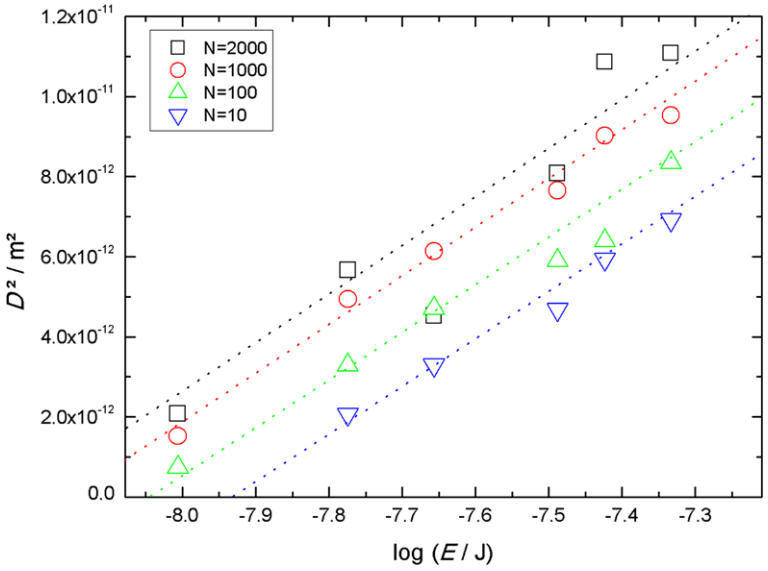

Fig. 4 Determination of thresholds for the ablation of the silicon substrate depending on the number of fs-laser pulses

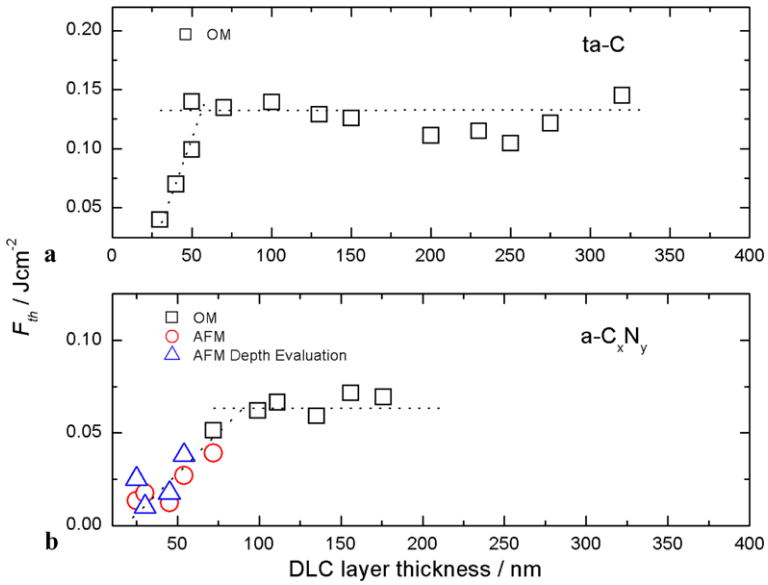

Fig. 5 F_{th} increases linearly with d for thicknesses $d < 60$ and $d < 90$ nm, depending on the DLC layer properties. When d exceeds this characteristic length, F_{th} becomes independent of d

The F_{th} values of the two phases, ta-C and a-C_xN_y (Fig. 5, Table 2) at high thicknesses are independent of the film thickness (0.120 J cm^{-2} and 0.065 J cm^{-2}). The ratio of these respective values is ca. 2, and can be modelled as follows:

$$\frac{F_{\mathrm{th}}(\text{ta-C})}{F_{\mathrm{th}}(\text{a-C}_x\text{N}_y)} = \frac{E_{\mathrm{sub}}(\text{ta-C}) \cdot l_{\mathrm{eff}}(\text{ta-C})}{E_{\mathrm{sub}}(\text{a-C}_x\text{N}_y) \cdot l_{\mathrm{eff}}(\text{a-C}_x\text{N}_y)}. \tag{10}$$

When we make the crude assumption that E_{sub} of the two materials is the same, the F_{th} ratio becomes simply equal to the ratio of the respective l_{eff} values:

$$\frac{F_{\mathrm{th}}(\text{ta-C})}{F_{\mathrm{th}}(\text{a-C}_x\text{N}_y)} = \frac{l_{\mathrm{eff}}(\text{ta-C})}{l_{\mathrm{eff}}(\text{a-C}_x\text{N}_y)}. \tag{11}$$

Now, the contributions to l_{eff} have to be identified according to (8). α_0 can be assumed similar for the two species. Radiation penetration depth values derived from low-energy spectroscopic ellipsometry data can only be correlated with the defect term, $\sigma_i N_i$, because nonlinear contributions, i.e. α_{NL}, cannot take place in ellipsometric measurements.

At $N = 1$ on a-C_xN_y, an α_{eff} of ca. 9×10^4 cm^{-1} could be derived from our evaluations by using (6), which corresponds to an effective penetration depth of the laser radiation, $\alpha_{\mathrm{eff}}^{-1} = l_{\mathrm{eff}}$, of ca. 110 nm. This l_{eff} contrasts to a value of $l_{\mathrm{eff}} < 5000$ nm of an a-C_xN_y film with $y = 0.12$ measured at $\lambda = 800$ nm [37]. This suggests that in our case of a-C_xN_y species with $y = 0.26$, at least a two-photon process has to be assumed. The nonlinear contribution, α_{NL}, therefore becomes finite. This is supported by a low energy value

of $l_{\mathrm{eff}} < 330$ nm of an a-C_xN_y film with $y = 0.12$ measured at $\lambda = 400$ nm, which agrees in the order of magnitude with $l_{\mathrm{eff}} \approx 110$ nm determined here (Table 2). Therefore, a two-photon absorption may take place even though linear processes occur in parallel due to a minor $E_g < 1.55$ eV, what should favour one-photon absorption. Also the α_{NL} of ta-C has to be finite due to higher band gaps of $E_g \approx 1.8$–3.0 eV (Table 2) which are clearly above the applied laser photon energy of 1.55 eV. Again, a two-photon process may be presumed as in the a-C_xN_y film. Thus, (11) can be written as

$$\frac{F_{\mathrm{th}}(\text{ta-C})}{F_{\mathrm{th}}(\text{a-C}_x\text{N}_y)} = \frac{\sigma_i N_i(\text{a-C}_x\text{N}_y) + \alpha_{NL}(\text{a-C}_x\text{N}_y)}{\sigma_i N_i(\text{ta-C}) + \alpha_{NL}(\text{ta-C})}. \tag{12}$$

Since $\sigma_i N_i(\text{ta-C}) \ll \sigma_i N_i(\text{a-C}_x\text{N}_y)$, the assumption of $\alpha_{NL}(\text{ta-C}) \approx \alpha_{NL}(\text{a-C}_x\text{N}_y)$ would lead to an extremely high threshold ratio, therefore $\alpha_{NL}(\text{a-C}_x\text{N}_y)$ must be greater than $\alpha_{NL}(\text{ta-C})$, which is supported by the higher band gap of ta-C in need for multiphoton absorption.

The ablation model of (6) is only based on an optical penetration depth of radiation, $\alpha_{\mathrm{eff}}^{-1}$, according to the Beer's law. The affected zone for modification/evaporation, however, may not only be constituted by the optical contribution, $\alpha_{\mathrm{eff}}^{-1}$ (7), but also by the additional emergence lengths of ballistic hot electrons out of the optical absorption zone, l_{ball}, and the heat diffusion length, l_T (controlled by τ_e, (2)), adding to a total affected zone, l_{tot}:

$$l_{\mathrm{tot}} = \alpha_{\mathrm{eff}}^{-1} + l_{\mathrm{ball}} + l_T, \tag{13}$$

so that (6) can be extended to

$$d = l_{\mathrm{tot}} \ln\left(\frac{F_0}{F_{\mathrm{th}}}\right). \tag{14}$$

In contrast to metals such as gold (cf. [25]), $l_{\mathrm{ball}} \ll \alpha_{\mathrm{eff}}^{-1}$ because of the strong electron–phonon coupling in ta-C and a-C_xN_y, i.e. low τ_e. With a carrier diffusivity $D_c = 0.2\ \mathrm{cm^2\,s^{-1}}$ [30, 38, 39] and a $\tau_e = 220$ fs [30], one calculates l_{ball} of ~2 nm for ta-C. To estimate also l_T, one can calculate a thermal diffusivity $D = 0.05\ \mathrm{cm^2\,s^{-1}}$ with a thermal conductivity of $\kappa = 0.1\ \mathrm{W\,cm^{-1}\,K^{-1}}$ [40] for ta-C films using the a density of $\rho = 3.0\ \mathrm{g\,cm^{-3}}$ [29] and a thermal capacitance of $C_p = 0.71\ \mathrm{J\,g^{-1}\,K^{-1}}$ [1] according to

$$D = \frac{\kappa}{C_p \cdot \rho}. \tag{15}$$

The electron–phonon relaxation time, τ_e, for ta-C, was determined to be 220 fs [30]. With these values, an l_T of ~1.5 nm ($\ll \alpha_{\mathrm{eff}}^{-1}$) can be calculated according to (2). Thus, l_{ball} and l_T can be neglected and $l_{\mathrm{tot}} \approx \alpha_{\mathrm{eff}}^{-1}$. With (7), l_{tot} becomes

$$l_{\mathrm{tot}} \approx (\alpha_0 + \sigma_i N_i + \alpha_{NL})^{-1}. \tag{16}$$

When the film thickness h becomes less than l_{tot}, F_{th} depends on h (Fig. 5).

Since $\sigma_i N_i(\text{ta-C}) \ll \sigma_i N_i(\text{a-C}_x\text{N}_y)$ and $\alpha_{NL}(\text{ta-C}) \ll \alpha_{NL}(\text{a-C}_x\text{N}_y)$ as stated above (12), $l_{\mathrm{tot}}(\text{ta-C})$ should be greater than $l_{\mathrm{tot}}(\text{a-C}_x\text{N}_y)$. Therefore an h-dependence of F_{th} should be observed at higher h-values of the ta-C film. This effect however is masked by the simultaneous absorption of the Si-substrate at low h-values (F_{th} of ta-C and Si are practically the same), and its parallel ablation together with the films (Fig. 5a). The measured overall threshold starts to get visibly lowered when the silicon cannot be simultaneously ablated anymore. In the case of a-C_xN_y (Fig. 5b), the Si substrate stays intact at these parameters because F_{th} of a-C_xN_y is less than that of Si.

4 Conclusions

Single-pulse modification fluence thresholds were used to characterise the interdependence of optical, electronic and thermal penetration zones with the thickness of nanoscale ta-C and a-C_xN_y layers grown on silicon wafers by inverse pulsed laser deposition.

The semilogarithmic dependence of the modification depth on fluence is described by an effective absorption coefficient. This includes the linear temperature-dependent absorption coefficient of the pure material, a term mainly determined by light absorbing impurities, a contribution considering radiation-induced defects, and a multiphoton (nonlinear optical) absorption coefficient. An extension of the Beer's law in respect to contributions of not only optical penetration depths but also to an additional emergence length of ballistic hot electrons, and the additional heat diffusion length, is discussed. The results suggest that both the emergence length of ballistic hot electrons and the heat diffusion length are negligible in contrast to the nanosecond laser pulse case where the modification threshold reaches the bulk value for a layer thickness equal to the thermal diffusion length.

Single-pulse modification thresholds dependent on the a-C_xN_y films thicknesses were determined to be below 90 nm. Multiphoton processes govern the modification behaviour since linear absorptions of 800 nm photons exhibit penetration depths >3 µm. An effective penetration depth of the laser radiation in a-C_xN_y was of ca. 110 nm in accordance with two-photon absorption.

The thickness dependence of the ta-C film thresholds below 60 nm can be explained by the simultaneous absorption of the Si substrate and the film, whereas in the case of a-C_xN_y the Si substrate stays intact supported by SFM data.

The threshold fluences of the thick films corresponding to bulk values were $0.120\ \mathrm{J\,cm^{-2}}$ for ta-C and $0.065\ \mathrm{J\,cm^{-2}}$ for a-C_xN_y. Employing the concept that threshold fluences

can be related to the sublimation energy volume density, the effective optical penetration depth, and the assumption that the sublimation energy volume densities are the same, the threshold ratio becomes equal to the ratio of the respective penetration depths which are mainly determined by optical contributions of defects.

Acknowledgements The partial financial support of the "Stiftung Aktion Österreich-Ungarn für Wissenschafts- und Erziehungskooperation" is kindly acknowledged. The authors thank F. Aussenegg (Graz), D. Bäuerle (Linz), V. Konov (Moscow), R. Stoian (St. Etienne), and T. Szörényi (Szeged) for valuable discussions.

References

1. D. Bäuerle, *Laser Processing and Chemistry*, 3rd edn. (Springer, Berlin, 2000)
2. A. Miotello, P.M. Ossi (eds.), *Laser-Surface Interactions for New Materials Production: Tailoring Structure and Properties*. Springer Series in Materials Science, vol. 130 (Springer, Berlin, 2010)
3. K. Sugioka, M. Meunier, A. Piqué (eds.), *Laser Precision Microfabrication*. Springer Series in Materials Science, vol. 135 (Springer, Berlin, 2010)
4. B. Volkel, G. Kaltenpoth, M. Handrea, M. Sahre, C.T. Nottbohm, A. Kuller, A. Paul, W. Kautek, W. Eck, A. Golzhauser, Surf. Sci. **597**, 32–41 (2005)
5. A. Gölzhauser, W. Eck, W. Geyer, V. Stadler, T. Weimann, P. Hinze, M. Grunze, Adv. Mater. **13**, 803–806 (2001)
6. C. Ebm, E. Platzgummer, H. Loeschner, S. Eder-Kapl, P. Joechl, M. Kuemmel, R. Reitinger, G. Hobler, A. Koeck, R. Hainberger, M. Wellenzohn, F. Letzkus, M. Irmscher, J. Vac. Sci. Technol. B **27**, 2668–2673 (2009)
7. A. Gölzhauser, W. Geyer, V. Stadler, W. Eck, M. Grunze, K. Edinger, T. Weimann, P. Hinze, J. Vac. Sci. Technol., B **18**, 3414–3418 (2000)
8. L. Reimer, *Scanning Electron Microscopy: Physics of Image Formation and Microanalysis*, 2nd edn. Springer Series in Optical Sciences (Springer, Berlin, 1998)
9. A. Miotello, R. Kelly, Appl. Phys. A, Mater. Sci. Process. **69**, 67–73 (1999)
10. W. Kautek, M. Forster, in *Laser Precision Microfabrication*, ed. by K. Sugioka, M. Meunier, A. Piqué. Springer Series in Materials Science, vol. 135 (Springer, Berlin, 2010), pp. 189–214
11. S. Kuper, M. Stuke, Appl. Phys. B, Photophys. Laser Chem. **44**, 199–204 (1987)
12. W. Kautek, S. Mitterer, J. Krüger, W. Husinsky, G. Grabner, Appl. Phys. A, Mater. Sci. Process. **58**, 513–518 (1994)
13. J. Krüger, W. Kautek, Laser Phys. **9**, 30–40 (1999)
14. C.R. Phipps (ed.), *Laser Ablation and Its Applications*. Springer Series in Optical Sciences, vol. 129 (Springer, New York, 2007)
15. J. Krüger, W. Kautek, Adv. Polym. Sci. **168**, 247–289 (2004)
16. W. Kautek, J. Krüger, M. Lenzner, S. Sartania, C. Spielmann, F. Krausz, Appl. Phys. Lett. **69**, 3146–3148 (1996)
17. M. Lenzner, J. Krüger, S. Sartania, Z. Cheng, C. Spielmann, G. Mourou, W. Kautek, F. Krausz, Phys. Rev. Lett. **80**, 4076–4079 (1998)
18. M. Lenzner, F. Krausz, J. Krüger, W. Kautek, Appl. Surf. Sci. **154**, 11–16 (2000)
19. E. Matthias, M. Reichling, J. Siegel, O.W. Kading, S. Petzoldt, H. Skurk, P. Bizenberger, E. Neske, Appl. Phys. A, Mater. Sci. Process. **58**, 129–136 (1994)
20. G. Daminelli, S. Pentzien, A. Hertwig, J. Krüger, Appl. Phys. A, Mater. Sci. Process. **83**, 89–94 (2006)
21. E. Matthias, J. Siegel, S. Petzoldt, M. Reichling, H. Skurk, O. Kading, E. Neske, Thin Solid Films **254**, 139–146 (1995)
22. S. Preuss, E. Matthias, M. Stuke, Appl. Phys. A, Mater. Sci. Process. **59**, 79–82 (1994)
23. Y. Hirayama, P.A. Atanasov, M. Obara, N.N. Nedialkov, S.E. Imamova, Jpn. J. Appl. Phys. Part 1 **45**, 792–797 (2006)
24. R.R. Fang, D.M. Zhang, H. Wei, Z.H. Li, F.X. Yang, X.Y. Tan, Chin. Phys. Lett. **25**, 3716–3719 (2008)
25. J. Krüger, D. Dufft, R. Koter, A. Hertwig, Appl. Surf. Sci. **253**, 7815–7819 (2007)
26. R. Koter, M. Weise, A. Hertwig, U. Beck, J. Krüger, J. Optoelectron. Adv. Mater. **12**, 663–667 (2010)
27. L. Egerhazi, Z. Geretovszky, T. Szorenyi, Appl. Phys. A, Mater. Sci. Process. **93**, 789–793 (2008)
28. T. Szorenyi, Z. Geretovszky, Thin Solid Films **453–454**, 431–435 (2004)
29. P. Boher, E. Fogarassy, T. Szorenyi, F. Antoni, Surf. Coat. Technol. **151**, 144–150 (2002)
30. E. Carpene, E. Mancini, C. Dallera, D. Schwen, C. Ronning, S. De Silvestri, New J. Phys. **9**, 404 (2007)
31. N. Matuschek, F.X. Kartner, U. Keller, IEEE J. Sel. Top. Quantum Electron. **4**, 197–208 (1998)
32. S. Baudach, J. Bonse, J. Krüger, W. Kautek, Appl. Surf. Sci. **154**, 555–560 (2000)
33. S. Gaspard, M. Forster, C. Huber, C. Zafiu, G. Trettenhahn, W. Kautek, M. Castillejo, Phys. Chem. Chem. Phys. **10**, 6174–6181 (2008)
34. G. Daminelli, J. Krüger, W. Kautek, Thin Solid Films **467**, 334–341 (2004)
35. N. Yasumaru, K. Miyazaki, J. Kiuchi, Appl. Phys. A, Mater. Sci. Process. **76**, 983–985 (2003)
36. G. Dumitru, V. Romano, H.P. Weber, S. Pimenov, T. Kononenko, M. Sentis, J. Hermann, S. Bruneau, Appl. Surf. Sci. **222**, 226–233 (2004)
37. L.K. Cheah, X. Shi, E. Liu, J.R. Shi, Appl. Phys. Lett. **73**, 2473–2475 (1998)
38. E. Staryga, G.W. Bak, Diam. Relat. Mater. **14**, 23–34 (2005)
39. S. Bhattacharyya, S.J. Henley, E. Mendoza, L. Gomez-Rojas, J. Allam, S.R.P. Silva, Nat. Mater. **5**, 19–22 (2006)
40. J. Robertson, Mater. Sci. Eng., R **37**, 129–281 (2002)
41. S.E. Rodil, S. Muhl, S. Maca, A.C. Ferrari, Thin Solid Films **433**, 119–125 (2003)